PCCP

PAPER

View Article Online
View Journal | View Issue

Cite this: *Phys. Chem. Chem. Phys.*, 2014, **16**, 12535

Flow dependent performance of microfluidic microbial fuel cells†

Daniele Vigolo,‡*[a] Talal T. Al-Housseiny,[b] Yi Shen,§[a] Fiyinfoluwa O. Akinlawon,[a] Saif T. Al-Housseiny,[c] Ronald K. Hobson,[d] Amaresh Sahu,[b] Katherine I. Bedkowski,[b] Thomas J. DiChristina[e] and Howard A. Stone*[a]

Received 13th March 2014,
Accepted 7th May 2014

DOI: 10.1039/c4cp01086h

www.rsc.org/pccp

The integration of Microbial Fuel Cells (MFCs) in a microfluidic geometry can significantly enhance the power density of these cells, which would have more active bacteria per unit volume. Moreover, microfluidic MFCs can be operated in a continuous mode as opposed to the traditional batch-fed mode. Here we investigate the effect of fluid flow on the performance of microfluidic MFCs. The growth and the structure of the bacterial biofilm depend to a large extent on the shear stress of the flow. We report the existence of a range of flow rates for which MFCs can achieve maximum voltage output. When operated under these optimal conditions, the power density of our microfluidic MFC is about 15 times that of a similar-size batch MFC. Furthermore, this optimum suggests a correlation between the behaviour of bacteria and fluid flow.

1 Introduction

Microbial fuel cells (MFCs) rely on the metabolic activity of bacteria to generate electricity. Although the electric capability of bacteria has been known for more than a century,[1] there has been a growing interest in understanding the fundamentals of this process and exploiting its applications. For example, several bacteria are able to consume nutrients and, in return, produce electrons and protons as metabolic products;[2] to name a few *Shewanella oneidensis* MR-1,[3,4] *Geobacter sulfurreducens* and *Pseudomonas aeruginosa*.[5] While electrons easily recombine in oxygen-rich water, they can be collected by electrodes in an anaerobic environment. The bacteria produce electrons and transfer them to the electrodes either (i) by direct contact, in which case bacteria adhere to electrodes and release electrons through their outer membrane[6] or through nanowires,[7] or (ii) by using mediators known as electron shuttles.[8–10] Typically, during this process, bacteria form colonies or a biofilm on the surface of the electrode.[11]

An MFC, as other fuel cells, consists of two compartments: the anode and the cathode. The electrons that are released by bacteria at the anode travel through an external circuit to the cathode, which closes the loop and produces an electric current. When the external circuit is loaded with a resistor, the electrical potential and current generated by the MFC can be measured. Most commonly, the anodic and cathodic compartments are separated by a cation-specific membrane to prevent electrons from migrating towards the cathode.[12] Conversely, in laminar co-flow MFCs,[13,14] the physical barrier, that is, the membrane, is not needed.

While MFCs present an alternative and an environmentally friendly energy source,[15,16] the main attraction of these systems is their dual use for both power generation and water treatment, since the microorganisms in MFCs can extract their nutrients from a vast range of waste water streams. For example, in the food industry,[17,18] waste streams are already populated with bacteria that can produce electricity.[15,19–21] Moreover, MFCs can be used as part of a decontamination process in large-scale waste water treatment; the byproduct electric power would be recovered.

Furthermore, MFCs can target specific hazardous contaminants, which are challenging to extract. For instance, *S. oneidensis* is able to reduce water-soluble uranium(VI) ions to insoluble uraninite ($U(IV)O_2$), allowing the decontamination of uranium-infested waters by simply collecting uraninite sediments.[22]

The ability to genetically modify bacteria can greatly expand the capabilities and benefits of MFCs, whose functions can be tailored for various applications. It is possible, for instance, to modify the genome of bacteria so that MFCs can, in addition to

[a] *Department of Mechanical and Aerospace Engineering, Princeton University, Princeton, NJ 08544, USA. E-mail: hastone@princeton.edu*
[b] *Department of Chemical and Biological Engineering, Princeton University, Princeton, NJ 08544, USA. E-mail: talal@princeton.edu*
[c] *School of Mechanical Engineering, Purdue University, West Lafayette, IN 47907, USA*
[d] *Morehouse College, Atlanta, GA 30314, USA*
[e] *School of Biology, Georgia Institute of Technology, Atlanta, GA 30332, USA*

† Electronic supplementary information (ESI) available. See DOI: 10.1039/c4cp01086h

‡ Present address: Department of Chemistry and Applied Biosciences, ETH Zürich, Vladimir-Prelog-Weg 1, 8093 Zürich, Switzerland. E-mail: daniele.vigolo@chem.ethz.ch

§ Present address: Institute of Food, Nutrition and Health, ETH Zürich, Schmelzbergstrasse 9, 8092 Zürich, Switzerland.

electricity generation, convert nutrients into high value chemicals such as ethanol[23] and biofuels.[24,25] Also, genetically modified bacteria and associated molecular reporters can be used to investigate the mechanisms responsible for electron transport in MFCs.

Even though the power generated by an MFC is typically quite low, the power density can reach reasonable levels of several hundreds to few thousands W m^{-3}, as in the present work and other notable studies.[26] This energy density is possible since most of the power is generated in the thin bacterial biofilm, which is of the order of tens of microns.[27] Therefore, it is beneficial to integrate MFCs into microfluidic devices,[12,28] where the cross-sectional length scale of the channels is also of the order of tens of microns. A number of studies have proposed various designs for microfluidic MFCs. However, most of the previous setups are batch processes[12,28–30] and only few studies consider continuously operated MFCs.[13,31] In addition to producing continuous uninterrupted current, the continuous flow feature enables MFCs to be supplied by passive flows such as capillary imbibition and gravity-driven drainage.

For continuous operation of microfluidic MFCs, the understanding of the influence of the flow of the electrolytic solutions is limited.[14] Pham *et al.*[32] investigated the effect of fluid flow on the biofilm and on MFCs performance. We note that the previous study was conducted in a fairly large chamber, which makes it challenging to control and characterize the interaction between fluid flow and the biofilm.

In the first part of this manuscript, we present the design of our continuous microfluidic MFC. Then, we report and analyse our experimental results obtained by varying the injection rate of the nutrient and catholyte solutions. Increasing the flow rate increases the delivery of nutrients to bacteria and may also stimulate the bacteria. On the other hand, at higher flow rates, *i.e.* higher wall shear stresses, the bacteria can be detached from the surface. We believe that these competing mechanisms are responsible for the optimal MFC performance, which we identify experimentally. Finally, we provide preliminary experiments that help us rationalize the flow dependent MFC voltage output.

2 Materials and methods

Our continuous MFC design, displayed in Fig. 1, consists of two identical compartments separated by a transparent, 183 μm thick, Nafion 117 (DuPont) proton exchange membrane (PEM). Our microfluidic MFC, which shares some similarities with the design of Qian *et al.*,[30] is operated in continuous mode as opposed to batch mode. Each compartment, representing either the anodic or the cathodic side of the cell, is composed of a serpentine microfluidic channel topped by a black, 190 μm thick, carbon paper (AvCarb MGL190), which acts as the electrode. We choose a serpentine configuration to maximize the surface to volume ratio in the two-dimensional microfluidic structure. In order to complete the circuit, the anodic and the cathodic carbon papers are connected by a thin electrical wire, which is loaded by an external resistor. We emphasize that the carbon paper we use offers several advantages, namely a surface roughness of about 8 μm and a high porosity of about 78%, which allows a larger number of bacteria to grow on the electrode.

The serpentine microfluidic channels, which are made in polydimethylsiloxane (PDMS) using standard soft lithography techniques,[33] are 200 μm in width and 100 μm in depth. Note that two consecutive serpentine loops are 100 μm apart. The total length of the serpentine channel is 17 cm and the overall area spanned by the channel is 10 mm by 5 mm. The electrical connection between the anode and the cathode is a thin stainless steel wire, which is 75 μm in diameter. The two PDMS microfluidic devices are punctured with a needle, in which the stainless steel wire is inserted in order for it to be in contact with the carbon paper. Then, when the needle is slowly removed, the wire remains trapped due to the elastic healing

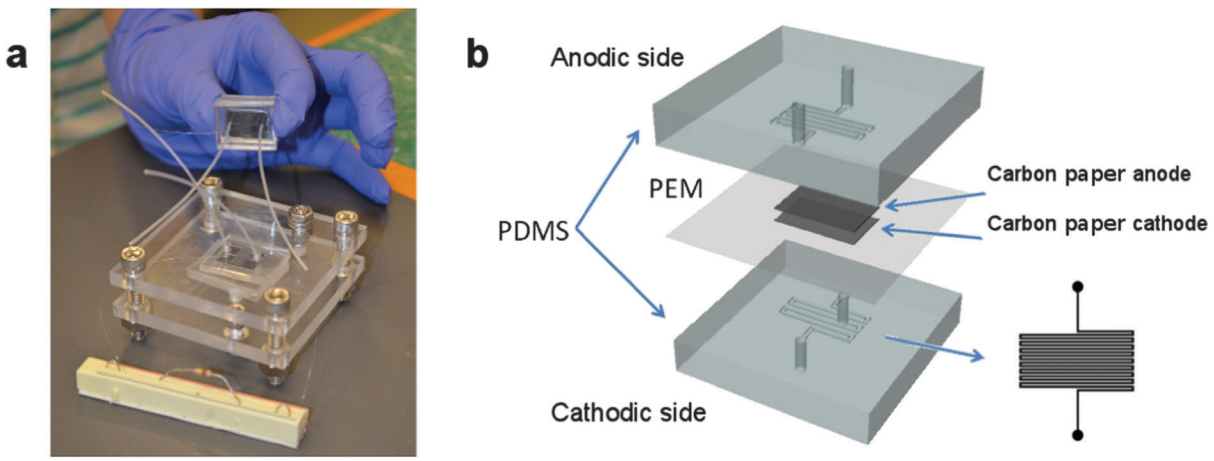

Fig. 1 The experimental design of our microfluidic MFC. (a) The two compartments of the MFC are sandwiched and held between fingertips. Underneath, we show a fully assembled MFC including a transparent plastic casing that houses the sandwiched PDMS compartments, flow tubing, and the external resistor (connected to the white strip). (b) A schematic of the experimental design, which is an accurate representation of the piece held between fingertips in (a).

of PDMS. Once the rectangular carbon paper is placed on top of the serpentine channel, the thin stainless steel wire is confined underneath the carbon paper to ensure good electrical contact. The other end of the wire is connected to a 100 kΩ resistor, which is the resistance we use throughout our study, unless stated otherwise. As shown in Fig. 1b, the two compartments, which are each composed of a serpentine microfluidic channel and a carbon paper electrode, sandwich the transparent PEM. In each compartment, the thin rectangular carbon paper is framed with an equally thin PDMS layer to prevent leakage in the horizontal direction. Finally, we use 1 mm Tygon tubings to supply the nutrient and the catholyte solutions to the microfluidic channels. The same type of tubing is used for the outlet connections.

Our MFCs experiments are conducted using the wild-type bacterial strain *S. oneidensis* MR-1. These microorganisms are facultative anaerobes. In anaerobic conditions, they can reduce metal ions such as Fe(III).[34] In the presence of small amounts of oxygen, as it is the case of our microfluidic experiments, these bacteria scavenge the oxygen and then act as in anaerobic conditions.

We first grow *S. oneidensis* aerobically overnight on a lysogeny broth (LB) plate in an incubator at 30 °C. Second, a few of the bacterial colonies are grown overnight in a 5 ml nutrient solution of tryptic soy broth (TSB). For this second step, the incubator is set at 30 °C and shaken at 100 rpm. Two hours before we start an experiment, the bacterial solution is allowed to cool down to room temperature after being diluted to a concentration of OD = 0.5, as evaluated by an IR-visible spectrophotometer set at a wavelength of 600 nm.

To start our experiments, we first flush the top microfluidic channel with a fresh TSB solution. The bottom channel is flushed with a phosphate-buffered potassium ferricyanide catholyte solution, $K_3Fe(CN)_6$ (50 mM in 100 mM phosphate buffer, pH 7.0). Once the top and bottom microfluidic channels are pre-wet, we slowly inoculate the top microchannel with 200 μL of the bacterial solution described above. Thus, the top compartment is always the anodic side by default. This configuration allows the bacteria to settle by gravity onto the porous carbon paper, which provides a scaffold for the formation of the biofilm. Following the inoculation process, we wait 15 minutes and then we inject the TSB and catholyte solutions into the anodic and the cathodic channels, respectively. These solutions are simultaneously supplied at a flow rate Q using the same syringe pump (Harvard Apparatus PHD 2000). Once we initiate the injection process, the voltage drop across the MFC is measured using a data acquisition board (National Instrument NI-BNC 2110), which is connected to a computer where one data point, *i.e.* voltage, is recorded every 20 s. We note that each MFC is used for one experiment only, and we always perform 3 to 6 identical experiments in parallel.

We performed a large number of experiments to examine the effect of the flow rate Q on the performance of our microfluidic MFC. With the exception of Q, all the experimental protocols, solutions, parameters and techniques are invariant throughout the present study. We note that the flow rate is held constant over the life of any experiment we conduct. We performed experiments with Q = 0.5, 2, 5, 10, 15, 20, 25, 30, 45, 60 μL min^{-1}. The wall shear stress is given by $\sigma_s \simeq 6\,\mu Q/(WH^2)$, where W and H are, respectively, the width and the height of the microchannel, and μ is approximately the viscosity of water. Hence, the range of the wall shear stress σ_s is 0.025–3 Pa.

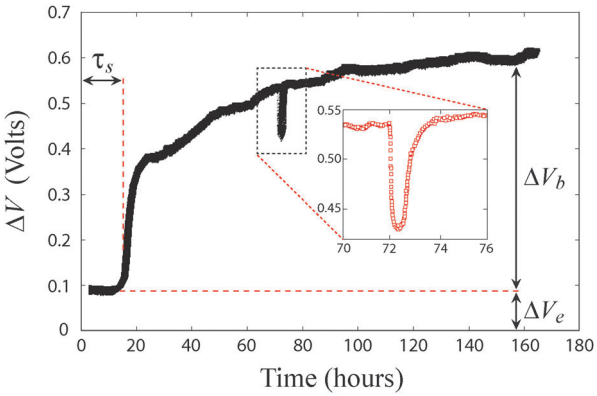

Fig. 2 A typical voltage curve for our microfluidic MFC. The experiment is conducted with a flow rate Q = 10 μL min^{-1}. The figure identifies the parameters that we study. The background electrochemical voltage is $\Delta V_e \approx 0.1$ V. The initial lag time before the bacteria start producing electricity is τ_s = 15 hours. The voltage due to bacterial activity reaches a plateau $\Delta V_b \approx 0.48$ V. In the inset, we show a blowup of the short-lasting voltage dip, which occurs when the flow is stopped and the syringes are being replenished.

A typical voltage curve for a microfluidic MFC experiment, where Q = 10 μL min^{-1}, is given in Fig. 2. One consistent signature of the measurements is that all experiments have a background voltage ΔV_e, which is an electrochemical potential that is not due to bacteria. In the next section, we show that ΔV_e varies with the flow rate Q. Also, the bacteria become active in producing electricity after a lag time τ_s, when the measured voltage starts to depart from ΔV_e. The voltage due to bacteria continues to increase in time until it reaches a roughly constant value denoted by ΔV_b, as indicated in Fig. 2. We found that the time it takes the MFC to reach the plateau ΔV_b is similar across all our experiments; it is of the order of 150–160 hours.

During the course of our experiments, we need to refill the two syringes containing the TSB and the catholyte solutions. This disturbance causes a transient dip in the voltage curve, as shown in the inset of Fig. 2. The replenishment of the syringes is reasonably fast (20 minutes) and does not disturb the bacterial activity. In fact, the value of the voltage drop before and after the refilling procedure is the same (Fig. 2). It is also important to note that the dip in voltage due to flow disruption is equal to ΔV_e, which confirms that ΔV_e is a flow-induced electrochemical potential.

3 Results and discussion

In the previous section, we defined the primary parameters that characterize the microfluidic MFC, namely the lag time τ_s before bacteria start contributing to the voltage, the background

electrochemical potential ΔV_e, and the maximum voltage produced by bacteria ΔV_b. We now report and explain the dependence of these parameters on the injection rate Q.

3.1 The background electrochemical potential ΔV_e

To accurately measure the background potential ΔV_e, we conduct a series of experiments in our MFC system in the absence of bacteria. The setup of these experiments is identical to the one described in the Materials and Methods section. In particular, the TSB and the electrolyte are injected at the same flow rate Q, and we measure the voltage drop for different values of Q. The voltage ΔV_e results from electrochemical reactions between the catholyte solution and the TSB solution. As shown in the inset of Fig. 3, ΔV_e increases with Q such that $\Delta V_e \propto Q^{1/3}$.

The dependence of the electrochemical potential on flow rate is not a feature that is unique to microfluidic MFCs. It is present in systems, which possess both electrochemical reactions and fluid flow, such as redox flow cells,[35–39] laminar co-flow fuel cells[40–43] and electrochemical reactions in packed bed reactors.[44] Even though it is not the main objective of our work, we need to characterize, and if possible understand, the dependence of ΔV_e on Q in order to evaluate the biological performance of MFCs, given that ΔV_e is contributed by flow electrochemistry rather than the bacteria. Next, we derive the $Q^{1/3}$ dependence using transport arguments, which are independent of the presence of bacteria.

Let us consider the flow of an electrolytic solution of concentration c_0 in a rectangular channel, where one of the four sides is an electrode. In this geometry, it is convenient to use a cartesian coordinate system. We take the height of the channel H to be along the y-axis, the width W along the z-axis, and the length L along the x-axis, which is the flow direction.

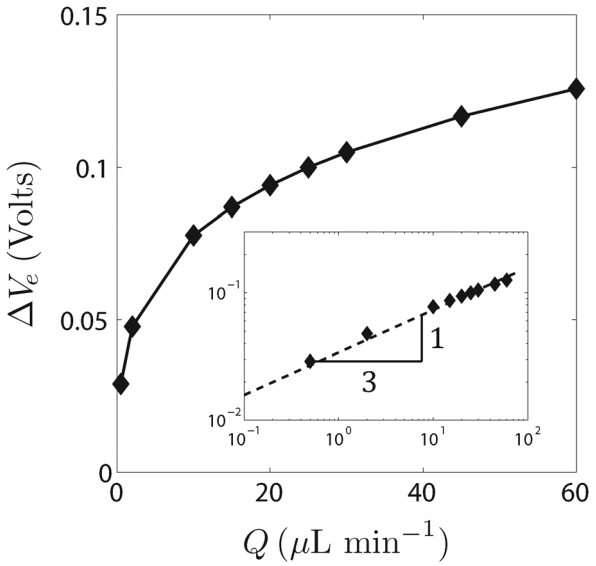

Fig. 3 The background electrochemical potential ΔV_e increases with the injection rate Q. The experiments are conducted in the absence of bacteria. The inset represents a log–log version of the main plot to highlight that $\Delta V_e \propto Q^{1/3}$.

Consistent with our design, we impose that $H \ll W \ll L$ and that the electrode is located at $y = 0$. We assume that the generated current is limited by the flux q of electrochemical reactants through the depletion layer along the electrode.[42,45,46] Since voltage drop is proportional to current by Ohm's Law and current, in its turn, is proportional to the flux q by Faraday's Law, we deduce that ΔV_e scales with the flux through the depletion layer q. Hence, our objective is now to demonstrate that $q \propto Q^{1/3}$, which is a familiar result in the literature on mass transfer.[48]

First, we can write a mass balance on any given tracer, which is transported by convection and diffusion. Assuming a steady-state fluid flow, the concentration of an electrochemical reactant c is described by

$$\boldsymbol{u}\cdot\boldsymbol{\nabla} c = D\nabla^2 c, \tag{1}$$

where $\boldsymbol{u}$ is the velocity vector of fluid particles, and D is the mass diffusivity. Here, we neglect electrical effects on the transport of ions.

Since we are interested in the flux towards the electrode, *i.e.* the carbon paper, the flow in the neighbourhood of this boundary can be approximated by a shear flow. Thus, the fluid velocity is expressed as $\boldsymbol{u} = \dot{\gamma} y\, \boldsymbol{e_x}$, where $\dot{\gamma} \simeq 6Q/(WH^2)$ is the wall shear rate for a rectangular channel. This unidirectional velocity satisfies the no-slip condition at the electrode $y = 0$. Using the previous approximation for the fluid velocity field, along with the separation of length scales $H \ll W \ll L$, eqn (1) reduces to

$$\dot{\gamma} y \frac{\partial c}{\partial x} = D\frac{\partial^2 c}{\partial y^2}. \tag{2}$$

We note that eqn (2) can be solved analytically with the appropriate boundary conditions.[43,47–49] However, this is not necessary here because we are seeking a scaling dependence. Since $\dot{\gamma} \propto Q$, a scaling analysis of eqn (2) shows that

$$\delta \propto \left(\frac{D}{\dot{\gamma}}x\right)^{1/3} \propto Q^{-1/3}, \tag{3}$$

where $\delta(x)$ is the thickness of the depletion layer[45,50] along the streamwise direction x. Inserting eqn (3) into the definition of the flux q, we arrive at

$$q = -D\frac{\partial c}{\partial y} \propto \frac{Dc_0}{\delta} \propto Q^{1/3}. \tag{4}$$

We point out that this result $\Delta V_e \propto q \propto Q^{1/3}$ is analogous to the classical Lévêque result,[51] which describes the thermal boundary layer resulting from a shear flow over a heated plate. We infer from eqn (4) that, owing to the 1/3 power-law dependence, increasing the flow rate beyond a certain level only contributes incrementally to the generated current.

The Lévêque scaling[51] (1928) stems from the theory of thermal boundary layers. In 2000, the Lévêque layer $\delta(x)$ was studied for laminar co-flows in microfluidic channels.[45] The previous study was beneficial to understand depletion layers in microfluidic co-flow fuel cells,[42,46] which were introduced[40,41] shortly after in 2002. However, and to the best of our knowledge, the connection between the depletion layer and the generated

current [eqn (3) and (4)], was only established recently (2013) in the co-flow fuel cell literature.[43,50] The Lévêque analysis and the associated scalings herein apply to MFC systems with flowing electrolytes such as industrial-scale packed bed MFCs,[52–54] micro-scale MFCs,[12,28–30,55] and microfluidic co-flow MFCs.[13,14,31,56]

3.2 The lag time τ_s

We next report the dependence of the lag time τ_s on the injection rate Q (see Fig. 4); our data exhibit systematic trends. For example, in the range $0 < Q < 15$ μL min^{-1}, the higher the flow rate, the earlier bacteria contribute to the voltage drop; τ_s decreases by a factor of 2 for an order of magnitude increase in Q. For larger flow rates, $Q > 15$ μL min^{-1}, τ_s is roughly constant within the experimental error margins.

Based on the trend we observe in Fig. 4, the bacteria start to generate electricity faster when subjected to higher flow rates. This phenomenon shows the direct responsiveness of our system to flow rate. As we will see in the next section, the transition at $Q \approx 15$ μL min^{-1} to the roughly constant τ_s regime that is maintained up to 60 μL min^{-1}, also corresponds to a maximum in the electrical output of our microfluidic MFC. The possible mechanisms responsible for this behaviour are also discussed.

3.3 The maximum bacterial voltage ΔV_b

The dependence of the bacterial voltage ΔV_b on the flow rate Q features a trend we find surprising. As shown in Fig. 5, ΔV_b increases with Q at lower rates and then decreases at higher rates. To thoroughly verify this trend, each data point in Fig. 5 represents at least four repetitions of the same experiment. This trend indicates an optimum flow rate range, $Q_{opt} = 15$–20 μL min^{-1}, for which $\Delta V_b \approx 0.57$ V is the maximum. We note that this value is achieved for a resistance $R = 100$ kΩ. As we will see later, our MFC power output is maximum for $R = 49$ kΩ, which corresponds to an even higher ΔV_b. The dependence of ΔV_b on the load has been noted in previous studies.[57] This dependence on the load is independent of the flow dependent performance of our MFC, which operates optimally under given flow rate conditions.

As observed in Fig. 4, the bacteria contribute to the measured voltage faster at higher flow rates. Hence, the shear stress could be playing the role of a stimulant. In addition, the supply of nutrients to bacteria increases with flow rate. On the other hand, high flow rates produce higher wall shear stresses that can lead to the detachment of bacteria from the carbon paper. This effect reduces the bacterial contribution to the current production. This would explain the sharp decrease in ΔV_b for $Q > 45$ μL min^{-1}.

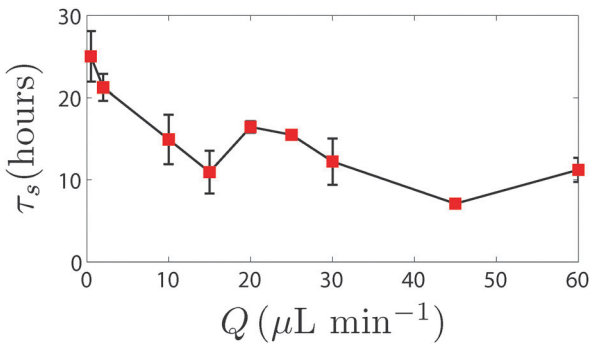

Fig. 4 The effect of the flow rate Q on the lag time τ_s, which is the time required for bacteria to start contributing to the voltage drop.

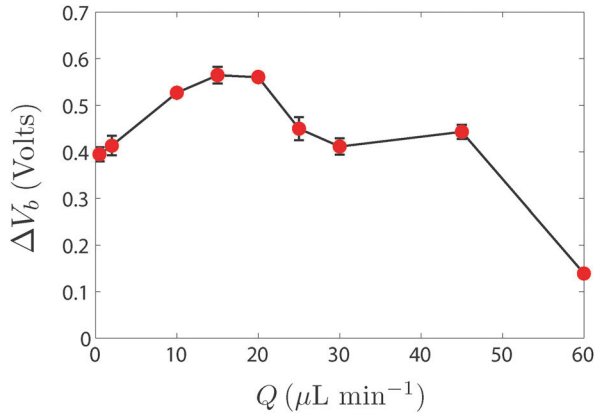

Fig. 5 The maximum voltage contributed by bacteria ΔV_b as a function of the flow rate Q. This measurement does not include the background electrochemical potential ΔV_e.

It is known that fluid flow influences the adhesion of bacteria on surfaces.[58–60] To further investigate the effect of flow, we performed experiments where we track over time the surface coverage of bacteria. We monitored the behaviour of *S. oneidensis* in the presence of TSB flow in the same serpentine channels that we used in our MFC experiments. To permit visualization by optical microscopy, we substitute the carbon paper with a glass substrate. Images were acquired every 5 minutes. As displayed in Fig. 6, we track the biofilm evolution for three different flow rates. The first case is below the optimal flow rate at 2 μL min^{-1}. The second case is around the optimal flow rate at 10 μL min^{-1}, and the third case is above at 45 μL min^{-1}. For 2 and 45 μL min^{-1}, the biofilm builds up in time until all the surface of the channel is covered with bacteria. We can observe that the surface coverage, for the full extent of the experiment, is minimal at 10 μL min^{-1}, which is near the optimal flow rate identified above.

The aim of the experiments conducted on glass surfaces is to understand the influence of the flow on the structure of the biofilm formed by *S. oneidensis*. The mechanisms of release and collection of electrons are complex and depend on several factors, which can be studied with specific experiments designed to elucidate each parameter. The previous experiments do not use rough electroactive substrates as in carbon paper. Nonetheless, they unveil a peculiar behaviour of bacteria under certain flow conditions. Although we cannot be certain, these experiments indicate that a similar behaviour might be taking place in our MFC experiments.

Bacteria form their biofilm as a defence mechanism to resist, for example, antibiotics.[61] Furthermore, it is well known that, when bacteria are assembled in a biofilm, their metabolic activity is different from planktonic cells of the same species.[62]

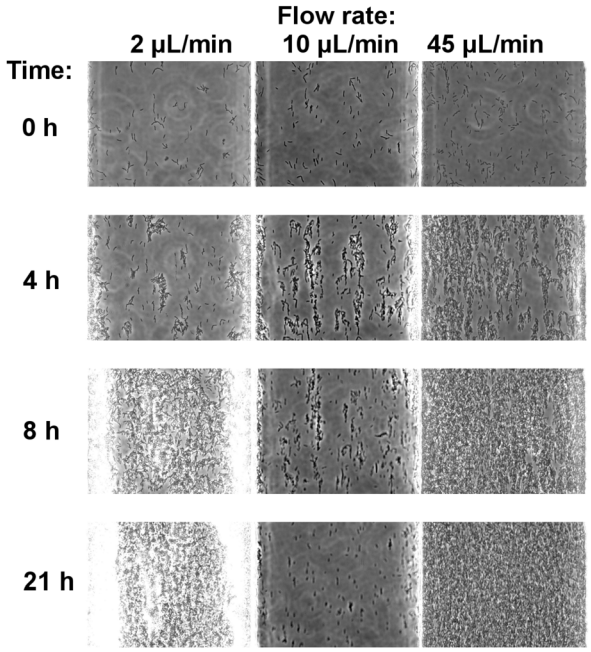

Fig. 6 The time evolution of surface coverage of bacteria for different flow rates Q. The experiments were performed using *S. oneidensis* MR-1 bacteria and serpentine microfluidic channels identical to those used in the MFC experiments. In contrast with MFC experiments, these surface coverage experiments were conducted on glass substrates rather than carbon paper so that we could visualize the bacteria using optical microscopy.

In fact, mass diffusion through the biofilm limits the transport of nutrients and the elimination of toxins produced by the bacteria.[63] In addition, the close proximity between bacteria and their interactions can influence their metabolic activity.[64] Here we speculate that, when subjected to an optimal shear stress, bacteria prefer to reduce the production of biofilm matrix. As a consequence, the aggregation of bacteria on the electrode (per unit area) as well as their energy consumption are reduced. Less aggregation increases the supply of oxygen and enables the bacteria to better dispose of their waste and toxins. These effects would yield the release of more electrons per bacterium.

It is also important to note that *S. oneidensis* can transfer electrons not only by direct contact, but also by releasing flavins, which are electrons shuttles.[10] Hence, the correlation between power generation and the experimental results of biofilm coverage on glass surfaces suggests that electron shuttles may become a more dominant mode of electron transfer under the optimal flow conditions. In this case, bacteria suspended in solution contribute the majority of electrons. In the absence of a dense biofilm at the optimal flow rate, it is less likely for electron shuttles to be slowed down or recombined in the biofilm since they would be able to readily reach the surface of the anode, which increases their intrinsic efficiency.

Further investigation is certainly needed to confirm the hypothesis presented above. To this end, we suggest conducting similar surface coverage experiments on carbon paper rather than glass. Such experiments would provide the bacteria with the same surrounding environment as our microfluidic MFC experiments. We note that the proposed experiments are not straightforward. For real-time visualization of biofilm build up, fluorescent bacteria are needed given the opaque nature of carbon paper. The latter requirement involves gene modification, which should have no effect on the electron release mechanism. In addition, the quenching of fluorescence might pose a challenge for long lasting experiments as in our MFC experiments.

In any case, there might be a connection between the optimum we identify and favourable shear stresses, which influence biofilm formation. The presence of flow is also favourable for the transport of nutrients to/from the biofilm. Moreover, the optimal flow rate might also account for the need of *S. oneidensis* MR-1 bacteria to scavenge oxygen, so that the released electrons are collected at the electrodes.

3.4 Power generation

Once the maximum voltage ΔV_b is reached for a given experiment, we can further characterize the MFC by its polarization curve; see Fig. 7. To generate this curve, we vary the resistance R of the steady state MFC and measure the corresponding voltage (V), current (I) and power (VI) across the cell. After 160 hours, the MFC reaches steady state. At that point, we change the resistor of the cell and wait at least three hours for the system to equilibrate. Then, we repeat this procedure to acquire more data points. Further details are provided in the ESI.† Note that the results in Fig. 7 account for the total potential drop across the MFC, that is, $\Delta V_b + \Delta V_e$.

We note that the maximum power $P \approx 4.5$ μW occurs at $R = 49$ kΩ, for which $V \approx 470$ mV and $I \approx 9.6$ μA. Although the absolute value of the voltage drop will change depending on the resistive load applied to the cell, the dependence on the flow rate, and the value of the optimal flow rate, should not be influenced by the value of the external load.

We now compare the performance of our MFC to similar studies. As a basis for comparison, we refer to the results of Qian *et al.*,[30] who had a similar MFC design operated in batch mode.

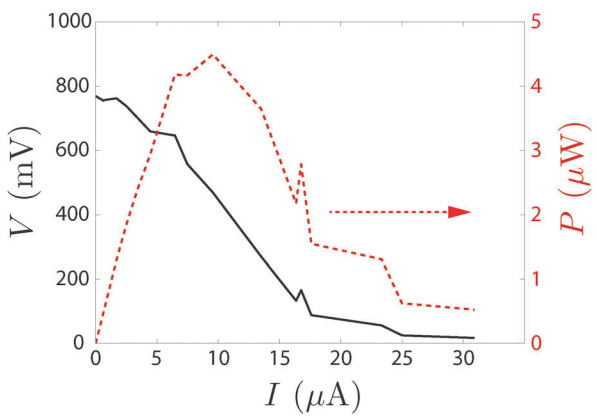

Fig. 7 The polarization curve for an MFC with $Q = 20$ μL min^{-1}. The voltage V, the current I, and the power $P = VI$ are obtained by varying the resistance R.

Table 1 Performance comparison between our continuous microfluidic MFC, a similar device operated in batch mode,[30] and a co-flow device.[13] All the MFCs are inoculated with the same bacteria *S. oneidensis* MR-1

	Qian *et al.*[30]	Li *et al.*[13]	Present work
Electrodes material	Carbon cloth	Cr and Au	Carbon paper
Nutrient medium	TSB	LB (Luria–Bertani)	TSB
Catholyte solution	$K_3Fe(CN)_6$	Phosphate buffer	$K_3Fe(CN)_6$
Anode volume (μL)	4	0.12	5
Anode area (mm^2)	40	1.4	50
Flow rate (μL min^{-1})	0 (batch-fed)	45	20
Shear stress (Pa)	0	6	1
Open circuit voltage (mV)	560	—	769
Max current (μA)	4	≈ 0.038	30.9
Max power (μW)	0.25	—	4.5
Max current surface density (mA m^{-2})	100	25.42	618
Max power density (W m^{-3})	62.5	—	900
Max power density (mW m^{-2})	6.25	—	90

They used the same *S. oneidensis* bacterial strain. The nutrient TSB solution and the $K_3Fe(CN)_6$ catholyte solution are also the same. It is clearly shown in Table 1 that, under the optimal flow rate conditions, the performance of our microfluidic MFC is very good. In particular, our power density is about 15 times higher than the power density reported by Qian *et al.*[30] This estimate is conservative since it accounts for the area of the entire carbon paper rather than the area of the serpentine channel alone. Furthermore, we compare in Table 1 the performance of our MFC with that of a co-flow MFC proposed by Li *et al.*[13] Despite that the latter work is a continuous flow setup, the resulting performance is much lower compared to our work. In particular, our current surface density is about 20 times higher than the value reported by Li *et al.*[13] Observe that comparing power densities is not possible since Li *et al.*[13] did not report voltage data. The previous data and comparisons demonstrate the important benefits of fluid flow, when applied optimally.

To showcase the capabilities of our MFCs, we connected in series four of our MFCs operating at the optimal flow conditions and powered up two simple electronic devices: a standard stopwatch and an LED (see ESI† for more details).

The objective of our work is not to maximize the power of MFCs. Rather, we seek to shed light on the effect of fluid flow on MFCs, so that we can push the boundaries of these systems by adding a new working parameter. In the presence of flow, existing MFCs can be further optimized since fluid flow can enhance the transport to nutrients, and can stimulate bacteria under an optimal range of shear stresses. We note that researchers have attempted several directions to increase the power output of MFCs,[65] such as varying the type of bacteria,[66,67] the material[66,67] and design[68] of electrodes.

4 Concluding remarks

The most common challenge facing microbial fuel cells is their low power output. On the other hand, their dual utility for water treatment and electricity generation is unique. In the present work, we show that integrating MFCs in a microfluidic device can improve their power density not only due to the high surface-to-volume ratio offered by the microfluidic geometry, but also by optimally tuning the flow conditions. In particular, we found that there is an optimal injection rate of the nutrient and the electrolyte for which our microfluidic MFC generate a maximum voltage drop. This optimal flow rate also yields the lowest operation lag time, which is the time required for the microorganisms in the MFC to start generating a voltage drop.

In the presence of flow, we note that bacteria are not the sole electrical source in MFCs. There is a flow-induced electrochemical potential ΔV_e, which is independent of bacteria and varies with the flow rate Q such that $\Delta V_e \propto Q^{1/3}$. It is essential to understand, describe and quantify this flow-induced electrochemical component in order to correctly distinguish it from the electrical contribution of bacteria.

To further investigate the optimal flow conditions, we introduce preliminary experiments, which exhibit an unexpected behaviour of the bacteria. At the optimal flow rate, the bacteria grow much less biofilm in comparison to lower and higher flow rates. In the presence of flow, a denser biofilm seems not to be a requirement for better power generation.

Acknowledgements

The authors thank the Princeton Grand Challenges program for financial support. We thank the NSF-REU program for hosting R. K. Hobson as part of a summer research program at Princeton. T. T. Al-Housseiny is supported by the National Science Foundation Graduate Research Fellowship under Grant No. DGE-0646086. T. DiChristina was supported by National Science Foundation Grants MCB-1021735 and EAR-0922243.

References

1 M. C. Potter, *Proc. R. Soc. London, Ser. B*, 1911, **84**, 260–276.
2 A. Rinaldi, B. Mecheri, V. Garavaglia, S. Licoccia, P. Di Nardo and E. Traversa, *Energy Environ. Sci.*, 2008, **1**, 417–429.
3 B. R. Ringeisen, E. Henderson, P. K. Wu, J. Pietron, R. Ray, B. Little, J. C. Biffinger and J. M. Jones-Meehan, *Energy Environ. Sci.*, 2006, **40**, 2629–2634.
4 T. J. DiChristina, J. K. Fredrickson and J. M. Zachara, *Rev. Mineral. Geochem.*, 2005, **59**, 27–52.
5 V. Sharma and P. P. Kundu, *Enzyme Microb. Technol.*, 2010, **47**, 179–188.
6 J. M. Myers and C. R. Myers, *Appl. Environ. Microbiol.*, 2001, **67**, 260–269.
7 Y. A. Gorby, S. Yanina, J. S. McLean, K. M. Rosso, D. Moyles, A. Dohnalkova, T. J. Beveridge, I. S. Chang, B. H. Kim, K. S. Kim, D. E. Culley, S. B. Reed, M. F. Romine, D. A. Saffarini, E. A. Hill, L. Shi, D. A. Elias, D. W. Kennedy, G. Pinchuk, K. Watanabe, S. Ishii, B. E. Logan, K. H. Nealson and J. K. Fredrickson, *Proc. Natl. Acad. Sci. U. S. A.*, 2006, **103**, 11358–11363.

8 M. E. Hernandez and D. K. Newman, *Cell. Mol. Life Sci.*, 2001, **58**, 1562–1571.
9 K. Rabaey and N. Boon, *Appl. Environ. Microbiol.*, 2004, **70**, 5373–5382.
10 H. von Canstein, J. Ogawa, S. Shimizu and J. R. Lloyd, *Appl. Environ. Microbiol.*, 2008, **74**, 615–623.
11 J. C. Biffinger, J. Pietron, R. Ray, B. Little and B. R. Ringeisen, *Biosens. Bioelectron.*, 2007, **22**, 1672–1679.
12 H.-Y. Wang, A. Bernarda, C.-Y. Huang, D.-J. Lee and J.-S. Chang, *Bioresour. Technol.*, 2011, **102**, 235–243.
13 Z. Li, Y. Zhang, P. R. LeDuc and K. B. Gregory, *Biotechnol. Bioeng.*, 2011, **108**, 2061–2069.
14 D. Ye, Y. Yang, J. Li, X. Zhu, Q. Liao, B. Deng and R. Chen, *Int. J. Hydrogen Energy*, 2013, **38**, 15710–15715.
15 B. E. Logan and K. Rabaey, *Science*, 2012, **337**, 686–690.
16 H. Wang, J.-D. Park and Z. Ren, *Environ. Sci. Technol.*, 2012, **46**, 5247–5252.
17 B. Cercado-Quezada, M.-L. Delia and A. Bergel, *Bioresour. Technol.*, 2010, **101**, 2748–2754.
18 X. Wang, Y. J. Feng and H. Lee, *Water Sci. Technol.*, 2008, **57**, 1117–1121.
19 M. M. Ghangrekar and V. B. Shinde, *Bioresour. Technol.*, 2007, **98**, 2879–2885.
20 H. Liu, R. Ramnarayanan and B. E. Logan, *Environ. Sci. Technol.*, 2004, **38**, 2281–2285.
21 A. Aldrovandi, E. Marsili, L. Stante, P. Paganin, S. Tabacchioni and A. Giordano, *Bioresour. Technol.*, 2009, **100**, 3252–3260.
22 M. J. Marshall, A. S. Beliaev, A. C. Dohnalkova, D. W. Kennedy, L. Shi, Z. Wang, M. I. Boyanov, B. Lai, K. M. Kemner, J. S. McLean, S. B. Reed, D. E. Culley, V. L. Bailey, C. J. Simonson, D. A. Saffarini, M. F. Romine, J. M. Zachara and J. K. Fredrickson, *PLoS Biol.*, 2006, **4**, 1324–1333.
23 M. D. Deng and J. R. Coleman, *Appl. Environ. Microbiol.*, 1999, **65**, 523–528.
24 S. K. Lee, H. Chou, T. S. Ham, T. S. Lee and J. D. Keasling, *Curr. Opin. Biotechnol.*, 2008, **19**, 556–563.
25 D. J. Sukovich, J. L. Seffernick, J. E. Richman, K. A. Hunt, J. A. Gralnick and L. P. Wackett, *Appl. Environ. Microbiol.*, 2010, **76**, 3842–3849.
26 S. Choi and J. Chae, *Sens. Actuators, A*, 2013, **195**, 206–212.
27 A. E. Franks, N. Malvankar and K. P. Nevin, *Biofuels*, 2010, **1**, 589–604.
28 F. Qian and D. E. Morse, *Trends Biotechnol.*, 2011, **29**, 62–69.
29 F. Qian, M. Baum, Q. Gu and D. E. Morse, *Lab Chip*, 2009, **9**, 3076–3081.
30 F. Qian, Z. He, M. P. Thelen and Y. Li, *Bioresour. Technol.*, 2011, **102**, 5836–5840.
31 J. W. Lee and E. Kjeang, *Biomicrofluidics*, 2010, **4**, 041301.
32 H. T. Pham, N. Boon, P. Aelterman, P. Clauwaert, L. De Schamphelaire, P. van Oostveldt, K. Verbeken, K. Rabaey and W. Verstraete, *Microb. Biotechnol.*, 2008, **1**, 487–496.
33 D. C. Duffy, J. C. McDonald, O. J. Schueller and G. M. Whitesides, *Anal. Chem.*, 1998, **70**, 4974–4984.
34 D. R. Lovley, D. E. Holmes and K. P. Nevin, *Adv. Microb. Physiol.*, 2004, **49**, 219–286.
35 C. Ponce de León, A. Fras-Ferrer, J. González-Garca, D. A. Szánto and F. C. Walsh, *J. Power Sources*, 2006, **160**, 716–732.
36 A. Z. Weber, M. M. Mench, J. P. Meyers, P. N. Ross, J. T. Gostick and Q. Liu, *J. Appl. Electrochem.*, 2011, **41**, 1137–1164.
37 R. E. Sioda, *Electrochim. Acta*, 1977, **22**, 439–443.
38 P. M. Lessner, F. R. McLarnon, J. Winnick and E. J. Cairns, *J. Appl. Electrochem.*, 1992, **22**, 927–934.
39 P. K. Leung, C. Ponce de León and F. C. Walsh, *Electrochem. Commun.*, 2011, **13**, 770–773.
40 E. R. Choban, L. J. Markoski, J. Stoltzfus, J. S. Moore and P. J. A. Kenis, *Power Sources Proc.*, 2002, **40**, 317–320.
41 R. Ferrigno, A. D. Stroock, T. D. Clark, M. Mayer and G. M. Whitesides, *J. Am. Chem. Soc.*, 2002, **124**, 12930–12931.
42 E. R. Choban, L. J. Markoski, A. Wieckowski and P. J. A. Kenis, *J. Power Sources*, 2004, **128**, 54–60.
43 W. A. Braff, M. Z. Bazant and C. R. Buie, *Nat. Commun.*, 2013, **4**, 2346.
44 J. Cano and U. Bohm, *Chem. Eng. Sci.*, 1977, **32**, 213–219.
45 R. F. Ismagilov, A. D. Stroock, P. J. A. Kenis, G. M. Whitesides and H. A. Stone, *Appl. Phys. Lett.*, 2000, **76**, 2376–2378.
46 E. Kjeang, N. Djilali and D. Sinton, *J. Power Sources*, 2009, **186**, 353–369.
47 L. G. Leal, *Advanced transport phenomena*, Cambridge University Press, 2007.
48 W. M. Deen, *Analysis of Transport Phenomena*, Oxford University Press, 1998.
49 W. Zhang, H. A. Stone and J. D. Sherwood, *J. Phys. Chem.*, 1996, **100**, 9462–9464.
50 W. A. Braff, C. R. Buie and M. Z. Bazant, *J. Electrochem. Soc.*, 2013, **160**, A2056–A2063.
51 M. A. Lévêque, *Ann. Mines*, 1928, **13**, 201.
52 K. Rabaey and W. Verstraete, *Trends Biotechnol.*, 2005, **23**, 291–298.
53 F. Davis and S. P. J. Higson, *Biosens. Bioelectron.*, 2007, **22**, 1224–1235.
54 Z. Du, H. Li and T. Gu, *Biotechnol. Adv.*, 2007, **25**, 464–482.
55 A. Fraiwan, S. Sundermier, D. Han, A. J. Steckl, D. J. Hassett and S. Choi, *Fuel Cells*, 2013, **13**, 336–341.
56 J. Yang, S. Ghobadian, P. J. Goodrich, R. Montazami and N. Hashemi, *Phys. Chem. Chem. Phys.*, 2013, **15**, 14147–14161.
57 P. Aelterman, S. Freguia, J. Keller, W. Verstraete and K. Rabaey, *Appl. Microbiol. Biotechnol.*, 2008, **78**, 409–418.
58 W. E. Thomas, E. Trintchina, M. Forero, V. Vogel and E. V. Sokurenko, *Cell*, 2002, **109**, 913–923.
59 S. Lecuyer, R. Rusconi, Y. Shen, A. Forsyth, H. Vlamakis, R. Kolter and H. A. Stone, *Biophys. J.*, 2011, **100**, 341–350.
60 A. Kumar, D. Karig, S. Neethirajan, A. K. Suresh, B. R. Srijanto, P. P. Mukherjee, S. Retterer and M. J. Doktycz, *ASME 3rd international conference on micro/nanoscale heat and mass transfer*, 2012, pp. 79–84.
61 P. S. Stewart and J. W. Costerton, *Lancet*, 2001, **358**, 135–138.

62 J. W. Costerton, Z. Lewandowski, D. E. Caldwell, D. R. Korber and H. M. Lappin-Scott, *Annu. Rev. Microbiol.*, 1995, **49**, 711–745.
63 N. Mozes and P. G. Rouxhet, *Biofilms – Science and Technology*, Springer, Netherlands, 1992, vol. 223, pp. 125–136.
64 M. Fletcher, *Biofilms – Science and Technology*, Springer, Netherlands, 1992, vol. 223, pp. 113–124.
65 H. Ren, H.-S. Lee and J. Chae, *Microfluid. Nanofluid.*, 2012, **13**, 353–381.
66 S. Choi, H.-S. Lee, Y. Yang, P. Parameswaran, C. I. Torres, B. E. Rittmann and J. Chae, *Lab Chip*, 2011, **11**, 1110–1117.
67 E. Parra and L. Lin, *IEEE 22nd international conference on micro electro mechanical systems*, 2009, pp. 31–34.
68 S. Inoue, E. A. Parra, A. Higa, Y. Jiang, P. Wang, C. R. Buie, J. D. Coates and L. Lin, *Sens. Actuators, A*, 2012, **177**, 30–36.